Constraining the ocean's biological pump with *in situ* optical observations and supervised learning. Part 2: Carbon Flux

D.J. Clements[1], S. Yang[1], T. Weber[2], A.M.P. McDonnell[3], R.Kiko[4], L.Stemmann[4], D.Bianchi[1]

[1]Department of Atmospheric and Oceanic Sciences, University of California Los Angeles, Los Angeles, CA, USA.
[2]Department of Earth and Environmental Sciences, University of Rochester,Rochester, New York, USA
[3]College of Fisheries and Ocean Sciences, University of Alaska Fairbanks, Fairbanks, Alaska 99775-7220, USA.
[4]Sorbonne Université, CNRS, UMR 7093, Institut de la Mer de Villefranche sur mer, Laboratoire d'Océanographie de Villefranche, Villefranche-sur-Mer, France.

Key Points:

- We use reconstructions of the global particle size distribution to estimate the particulate carbon export flux.
- We quantify the importance of particle size distribution slope and biovolume on the magnitude of the reconstructed fluxes.
- We show reduced spatial and temporal gradients relative to prior carbon export estimates.
- Fluxes estimated at two depths show that more carbon is exported from the wintertime mixed layer than the euphotic zone.

Corresponding author: D.J Clements, dclements@atmos.ucla.edu

Corresponding author: D. Bianchi, dbianchi@atmos.ucla.edu

Abstract

Export of sinking particles from the surface ocean is critical for carbon sequestration and for providing energy to the deep-ocean biosphere. The magnitude and spatial patterns of this flux have been estimated in the past by *in situ* flux observations, satellite-based algorithms, and ocean biogeochemical models; however, these estimates remain uncertain. Here, we use a novel machine learning reconstruction of global *in situ* ocean particle size spectra from Underwater Vision Profiler 5 (UVP5) measurements, to determine particulate carbon fluxes. We combine global maps of particle size distribution parameters for large sinking particles with observationally-constrained empirical relationships to calculate the sinking carbon flux from the euphotic zone and the wintertime mixed layer depth. Our flux reconstructions are comparable to prior estimates, but suggest a less variable seasonal cycle in the tropical ocean, and a more persistent export in the Southern Ocean than previously thought. Because our estimates are not bounded by a specific depth horizon, we reconstruct export at multiple depths, and find that export from the wintertime mixed layer globally exceeds that from the euphotic zone. Our estimates provide a baseline for more accurate understanding of particle cycles in the ocean, and open the way to fully three-dimensional global reconstructions of particle size spectra and fluxes in the ocean, supported by the growing database of optical observations.

1 Introduction

At the ocean surface, primary production and other biogeochemical processes interact to form organic particles that drive the ocean's biological pump (Volk & Hoffert, 1985; Honjo et al., 2008; Turner, 2015). Aggregation and sinking of particulate organic matter stores inorganic carbon and nutrients in the deep ocean for timescales ranging from decades to centuries (Boyd et al., 2019; DeVries et al., 2012), thus reducing surface carbon concentrations and leading to a decrease in atmospheric CO_2 (Kwon et al., 2009). Sinking particles provide the organic matter feeding the deep ocean fauna (Robinson et al., 2010; Siegel et al., 2014) and shape the ocean's microbiome (Karl et al., 1984; Fontanez et al., 2015; Bianchi et al., 2018).

Several studies have estimated the global particle export from the euphotic zone, resulting in a wide range of values – from less than 3 to more than 10 PgC/y (Henson et al., 2011; Siegel et al., 2014; DeVries & Weber, 2017; Dunne et al., 2007), with some of the discrepancies depending on the methods used (Quay et al., 2020). Biogeochemical models yield a global export of 4-6 PgC/y when tuned to match particle observations (Siegel et al., 2014), but can reach up to 10 PgC/y when tuned to match in situ profiles of nutrients and other biogeochemical tracers (DeVries & Weber, 2017). A similar range is suggested by recent global IPCC-class Earth System Models, which produce global carbon exports from 2.4 to 12 PgC/y, with an average of 7.4 Pg/y (Séférian et al., 2020). Data-driven estimates that combine satellite-based primary production with empirical estimates of particle export ratios often result in fluxes near the upper range (Dunne et al., 2007; Laws et al., 2011; Guidi et al., 2015), with some exceptions (Henson et al., 2011). A global export of around 10 PgC/y is comparable to biogeochemical estimates of annual net community production over the mixed layer (Emerson, 2013; Quay et al., 2020). However, on long timescales, community production is thought to be balanced by multiple export processes(Boyd et al., 2019) that also include subduction of non-sinking organic carbon (Carlson et al., 1994; Dall'Olmo et al., 2016) and vertical migrations of zooplankton and fish (Longhurst et al., 1990; Steinberg et al., 2000; Bianchi et al., 2013).

Besides large scale discrepancies in the total export, regional patterns of particle export predicted by these methods also vary substantially, with some models suggesting dramatic gradients between productive and oligotrophic waters (Dunne et al., 2007), and others suggesting more muted variations (DeVries & Weber, 2017). Differences in

regional export fluxes have been attributed to methodological limitations, including scarcity and variability of *in situ* data used to constrain models, variability in satellite-based primary production algorithms, and models not able to fully capture underlying physical and biological processes. Based on *in situ* geochemical observations, Quay et al. (2020) suggest a weaker meridional variability in export flux than prior estimates, stressing the need for expanding and combining observational approaches and models to fully constrain particle export patterns.

Recent studies have also highlighted the importance of standardized methods and metrics used to quantify particle export (K. O. Buesseler et al., 2020). In particular, the depth horizon of export has been identified as one of the leading causes of diverging estimates (Palevsky & Doney, 2018). Two choices of export horizon have been commonly adopted: the base of the euphotic zone, either as a variable depth or global average (K. O. Buesseler & Boyd, 2009; Siegel et al., 2016, 2014; Bisson et al., 2018; Dunne et al., 2007; DeVries et al., 2017; Henson et al., 2011), and the mixed layer depth, both as seasonally varying and maximum depth (Emerson, 2013; Quay et al., 2020). These choices underlie different interpretations of export fluxes: export from the euphotic zone provides an ecosystem-centric viewpoint, while export from the mixed layer provides an estimate of carbon storage. Export from the euphotic zone should balance net community production on long time scales (Emerson, 2013), and, since synthesis of new particles should be minimal below the euphotic zone, it should provide an upper limit to the energy that can fuel subsurface ecosystems. Carbon exported below the maximum mixed layer is removed from contact with the atmosphere for timescales longer than a year, and thus is relevant for long term carbon sequestration.

Export of particulate organic matter results from the combination of multiple physical and biological processes (Turner, 2015; Boyd et al., 2019). Gravitational settling of particles denser than seawater, including fecal pellets, phytodetritus, and heterogeneous aggregates, is thought to be the primary export mechanism, contributing to about 60% of the total carbon export, and about half of the carbon storage in the deep ocean (Boyd et al., 2019). Other processes, such as organic matter transport and repackaging by vertically migrating organisms (Longhurst et al., 1990; Bianchi et al., 2013; Kiko et al., 2020) and physical injection of dissolved and suspended particles (Carlson et al., 1994; Omand et al., 2015; Stukel et al., 2017; Dall'Olmo et al., 2016) make up the remainder (Boyd et al., 2019). Using both an euphotic viewpoint, and considering only gravitational settling, particle flux estimates have begun to converge on a value of 5-6 PgC/y (Palevsky & Doney, 2018; Boyd et al., 2019).

In the field, sediment traps and thorium deficit measurements have been used to quantify sinking particle fluxes. However, both types of observations lack substantial global coverage, vertical resolution, and have known biases, making extrapolations to global scale difficult (K. Buesseler et al., 2007; Le Gland et al., 2019). Recently, optical methods have gained traction to estimate particle export. These methods are based on *in situ* observations of particle size distribution (PSD), i.e., the particle abundance as a function of size (Guidi et al., 2008; Bourne et al., 2019). Among optical instruments, the Underwater Vision Profiler 5 (UVP5), measures the abundance of particles in the 80 μm - 2.6 cm range (Picheral et al., 2010) and is routinely deployed on oceanographic expeditions (Kiko et al., 2021). The high vertical resolution of UVP5 observations, combined with empirical, size-dependent relationships for carbon content and sinking speed (Kriest, 2002; Stemmann et al., 2004), enables a uniquely detailed view into the three-dimensional ocean particle flux (Guidi et al., 2016). Observations from UVP5 have been used to quantify particulate flux from the surface ocean on a regional basis (Guidi et al., 2008, 2009; Kiko et al., 2017; Cram et al., 2018; Forest et al., 2012), and to reconstruct export fluxes across large-scale biomes based on a limited set of measurements (Guidi et al., 2015). However, the growing database of UVP5 observations has not yet been used to quantify particle fluxes and their distribution at the global scale.

In this study, we combine a global reconstruction of PSDs from UVP5 observations with in situ particle flux observations to provide a new estimate of the magnitude and patterns of particle export. The global PSD reconstruction is described in a companion paper (Clements et al., 2021), and consists of a machine learning approach that predicts observed PSD from *in situ* UVP5 observations and well sampled environmental variables. These PSD distributions are then combined with empirical relationships that relate particle size and abundance to sinking fluxes (Kriest, 2002; Guidi et al., 2008; Kiko et al., 2017), which we tune against a global data set of *in situ* sediment trap and thorium-derived particle flux observations (Bisson et al., 2018). Although there are known biases in the trap and thorium flux data (K. Buesseler et al., 2007; Le Gland et al., 2019), they are currently the best estimates of *in situ* carbon flux. By comparing patterns in particle flux with potential environmental drivers, we gain insight into the mechanisms responsible for particle export and its spatial and temporal variability. Finally, we exploit the high vertical resolution of UVP5 measurements to estimate particle flux at both the climatological euphotic zone depth and the maximum mixed layer depth, revealing the importance of the export horizon for this quantity.

The rest of the paper is organized as follows. Section 2 describes the methods used to reconstruct particle fluxes from global PSD reconstructions and *in situ* carbon export observations. Section 3 presents the results of our export flux reconstructions, comparing them to previous studies at regional and global scales, and discussing the uncertainties and caveats inherent to our approach. Section 4 summarizes the main findings and future directions.

2 Methods

The flux of particulate carbon (ϕ, $\frac{mgC}{m^2 day}$) at any given depth can be expressed as a function of three size-dependent quantities: the number of particles of a given size, i.e., the PSD ($n(s), /frac\#m^3$), the sinking speed ($w(s)\frac{m}{s}$), and the carbon content of each particle ($c(s)$), according to the following equation (Guidi et al., 2008; Stemmann & Boss, 2012):

$$\phi = \int_{s_{min}}^{s_{max}} n(s) \cdot w(s) \cdot c(s)\, ds, \tag{1}$$

Here, s indicates the particle equivalent spherical diameter, or size, and s_{min} and s_{max} the minimum and maximum size of particles considered for export. We further assume that the quantities in Equation 1 can be approximated by power laws that depend on particle size, each characterized by an intercept (the size-independent coefficient) and a slope (the exponent for size-dependence) (Stemmann & Boss, 2012):

$$n(s) = n_0 \cdot s^{-\beta} \tag{2}$$

$$w(s) = w_0 \cdot s^{\eta} \tag{3}$$

$$c(s) = c_0 \cdot s^{\zeta}, \tag{4}$$

Thus, by using Equations 2-4, the total particle flux can be expressed as:

$$\phi = \int_{s_{min}}^{s_{max}} n_0 \cdot w_0 \cdot c_0 \cdot s^{-\beta+\eta+\zeta}\, ds = \int_{s_{min}}^{s_{max}} n_0 \cdot m_0 \cdot s^{-\beta+\mu}\, ds \tag{5}$$

where we combined the intercepts and exponents of the sinking speed and carbon content relationships by setting $m_0 = w_0 \cdot c_0$ and $\mu = \eta + \zeta$, following the approach by (Guidi et al., 2008). We further approximate m_0 and μ with globally constant values, which we constrain with *in situ* observations. In practice, we calculate the continuous integral in Equation 5 as a discrete summation over the finite size bins that approximate the PSD.

We use PSD properties (biovolume and slope) from a global UVP5-based reconstruction described in a companion paper, shown in figure 1 (Clements et al., 2021), and combine them with empirical relationships for sinking velocity and carbon content to estimate particle fluxes by solving Equation 5. Since the parameters that define the combined sinking speed and carbon content relationships, i.e., m_0 and μ, are relatively unconstrained, we optimized them by minimizing the mismatch between predicted particle fluxes and *in situ* observations from sediment traps and thorium-uranium disequilibrium (Section 2.1). We exploit the three-dimensional nature of UVP5 observations to estimate particle fluxes at two different export horizons: the base of the euphotic zone (here defined by the 1% light level following Morel et al. (2007)) and the annual maximum mixed layer depth (Johnson et al., 2012).

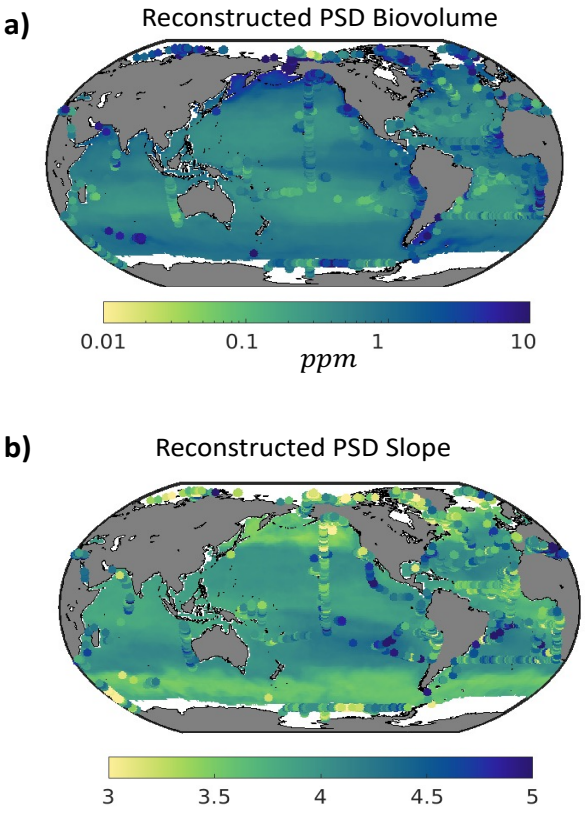

Figure 1. Global reconstructions of PSD biovolume (a) and slope (b) based on a machine-learning extrapolation of *in situ* UVP5 observations (Clements et al., 2021). Color contours show reconstructed variables as annual means. Dots show *in situ* quantities from UVP5 observations. Note that observations reflect specific months of the year, explaining some of the mismatch with the annual mean quantities shown by the background colors.

2.1 Sinking Speed and Carbon Content

Particle sinking speed and carbon content have been empirically evaluated using power law relationships analogous to Equations 3 and 4, e.g., as compiled in Kriest (2002) and Stemmann et al. (2004). Most of these studies measured a range of particles that does not wholly encompass the sizes detected by the UVP5. Furthermore, these relationships are defined for specific particle types, which are not distinguished in the PSD reconstruction used here (Clements et al., 2021).

Since estimates of total flux are sensitive to the sinking speed and carbon content relationships, here encapsulated by the parameters m_0 and μ, we apply an optimization procedure to keep our results consistent with *in situ* flux measurements. Specifically, we find the values of m_0 and μ that minimize the sum of the square errors between particle flux predictions (Equation 5) and co-located *in situ* carbon flux measurements (Bisson et al., 2018). We use both trap and thorium flux data, corrected to be at the euphotic depth, as described in Bisson et al. (2018). We average together all *in situ* data into a 1 degree global grid, by month, similar to the UVP5-based PSD reconstruction (Clements et al., 2021), so that the optimization reflects climatological conditions.

Because the size distribution of particles that contribute to the flux is poorly constrained, we perform this optimization for a range of plausible minimum and maximum sizes for Equation 5, selecting a physically reasonable combination for the final estimate. Ultimately, when optimizing the sinking carbon parameters, the total global export flux is not sensitive to the size range; however the resulting empirical relationships are (see Supplementary Fig. S1). The insensitivity of the carbon flux to the size range indicates a compensatory effect between the sinking carbon parameters and the size range selected for the optimizations. Thus, choosing different size combinations would result in a similar total flux, although it may slightly alter spatial or temporal patterns in a compensatory way.

Our final choice of size range is informed by average sinking speeds and carbon content previously reported (Kriest, 2002). Based on this optimization analysis, we set the minimum size class to be 35 μm, where the average sinking speed is near 1 m d^{-1} (Smayda, 1970; Kriest, 2002). Although it is lower than the detection limit of the UVP5, the power law slope can likely be extended to this size range (Stemmann & Boss, 2012). Most organic particles smaller than this size are likely rapidly remineralized, making their contribution to the sinking flux negligible (Riley et al., 2012). Even if some smaller particles could sink more rapidly (e.g., because of higher concentrations of mineral "ballast" and higher density) and could contribute more substantially to the total flux, neglecting them would not significantly affect our final results, because the optimized flux is nearly insensitive to the size range selected. We choose 5 mm as the maximum size, i.e., the same maximum size used for the PSD reconstructions (Clements et al., 2021), roughly corresponding to the size where zooplankton become important contributors to the particle biovolume detected by UVP5 in a variety of regions (Forest et al., 2012; Stemmann, Youngbluth, et al., 2008; Stemmann & Boss, 2012).

Overall, this optimization approach results in a value of 2.9 for the exponent μ, and 27.65 mgC m s^{-1} $cm^{-2.9}$ for the intercept m_0, both in the range suggested by *in situ* observations (Kriest, 2002), and comparable to values adopted by previous studies (Kriest, 2002; Stemmann et al., 2004; Guidi et al., 2008; Kiko et al., 2017; Bianchi et al., 2018).

2.2 Flux reconstruction and evaluation

We evaluate reconstructed particle export fluxes by comparing them to *in situ* flux observations and previous global reconstructions. Specifically, we compare total fluxes, zonal averages, and seasonal cycles. For these comparisons, we divide the ocean into 14 biogeochemically-consistent regions based on the boundaries identified by Weber et al.

(2016), with an additional boundary along the equator to separate Northern and Southern Hemispheres. We evaluate seasonal cycles by analyzing temporal correlations between reconstructions, and assessing their seasonal cycles.

We first present results for fluxes estimated at the climatological euphotic zone depth, and then repeat the calculation at the maximum mixed layer depth. This requires an estimate of the PSD at the maximum mixed layer depth, which we calculate from UVP5 observations following the same machine learning approach (a bagged Random Forest) used to estimate PSD at the euphotic zone depth, described in Clements et al. (2021). We keep the same sinking speed and carbon content parameters, assuming that they do not change substantially between the two depths, which are often not too far from each other. Thus, the only methodological difference between the two estimates is the depth of the PSD reconstruction used to calculate the flux. We quantify the error of our estimates by determining the standard deviation of 100 different Random Forest realizations that differ in the choice of predictor variables and hyperparameters (Clements et al., 2021).

3 Results and Discussion

3.1 Particle export fluxes

The resulting global carbon flux reconstruction compares well with *in situ* sediment trap and thorium-based observations (Fig. 2), performing in a similar way or better than previous estimates (Henson et al., 2011; Dunne et al., 2007; Siegel et al., 2014). Compared to previous work, our estimate reduces the overall uncertainty relative to observations, as expressed by the RMSE, and shows minimal bias. However, our method also reduces the overall range of reconstructed fluxes, i.e., it overestimates the flux at low values and underestimates it a high values compared to observations. This bias may be related to a similar underestimate of the range of PSD biovolume and slope that may be related to the specific machine learning method (a bagged Random Forest ensemble) used to extrapolate UVP5 observations (Clements et al., 2021). It is also possible that the optimization approach against an averaged global dataset of *in situ* fluxes fails to capture extremes in particle export at both the high and low range of observations.

Comparing sediment trap and thorium-based observations to the various estimates of Fig. 2 highlights the relative strengths and weaknesses of each approach. The results from Dunne et al. (2007), based on combining satellite primary production with empirical estimates of particle export ratios, match the observed values well, but tend to overestimate the larger fluxes (not shown in the figure). The estimate by Henson et al. (2011), based on a similar approach as Dunne et al. (2007), follows a similar pattern as observations, as indicated by the high r^2, but systematically underestimates the flux magnitude, as shown by the negative bias. The satellite-driven, model-based estimate from Siegel et al. (2014) captures the overall magnitude of export, but misses some of the variability of observations, as indicated by the relatively low r^2. Overall, all estimates in Fig. 2 show combinations of strengths and weaknesses, and it would be difficult to highlight a specific model as unconditionally superior. We suggest that a combination of estimates should be used to asses export of carbon from the surface ocean, and that future efforts should strive to reduce the biases discussed above, potentially combining strengths from different approaches.

Extrapolated to the whole ocean, our method reveals spatial patterns of export fluxes in broad agreement with previous studies, with some notable differences (Fig. 3). Similar to other estimates, particle fluxes tend to decrease from high to low latitudes, and from coastal regions to the open ocean. A local maximum of export is reproduced along the equator, and is particularly evident in the Pacific Ocean. Compared to previous work, our method produces somewhat weaker gradients between coastal and offshore waters,

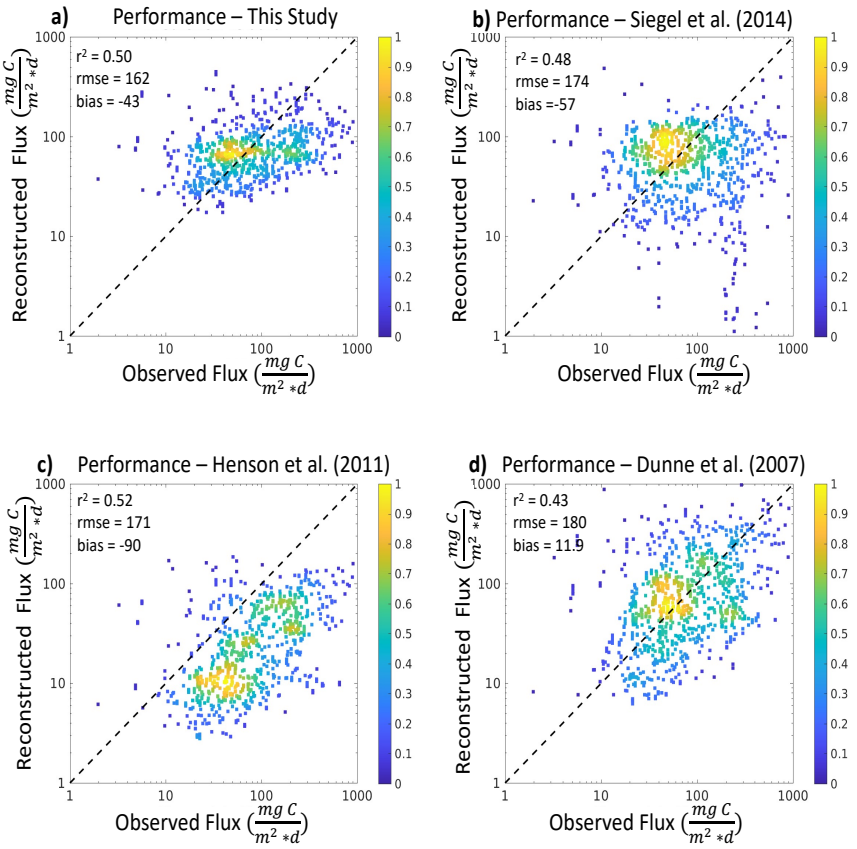

Figure 2. Density scatter plots showing the relationships between *in situ* flux observations and global flux reconstructions (mg C m^{-2} d^{-1}) at the base of the euphotic zone from (a) this study, (b) Siegel et al. (2014), (c) Henson et al. (2011), (d) (Dunne et al., 2007). Colored dots represent the relative density of grid points surrounding the data point, and the dashed line indicates a 1:1 ratio. Annotations show the coefficient of determination (r^2), RMSE, and average bias. Note that to keep similar x-axes and allow better comparison between the different estimates, a limited number of points with flux larger than 1000 mg C m^{-2} d^{-1} have been omitted from the figures.

with slightly higher fluxes near the centers of subtropical gyres, and suggests an asymmetry between the subpolar Atlantic and Pacific Oceans, with more intense particle export along the gulf of Alaska than in the North Atlantic (see also Section 3.1.1). We also reconstruct substantially stronger export than previously found in the Southern Ocean, in particular south of 50S (see discussion in Section 3.2).

Globally integrated, we estimate a particle export flux of 6.7 ± 0.4 PgC/y, in good agreement with the range of observational and model-based estimates of the biological gravitational pump (4-9 PgC/y, Boyd et al. (2019)). Compared to other spatially-resolved reconstructions, our global flux sits between the low-value estimate of Henson et al. (2011) (3.0 ± 0.3 PgC/y) and the high-value estimate of Dunne et al. (2007) (9.8 ± 0.4 PgC/y). Seasonal maps of the export and standard deviation are shown in Supplementary figures S2 and S3.

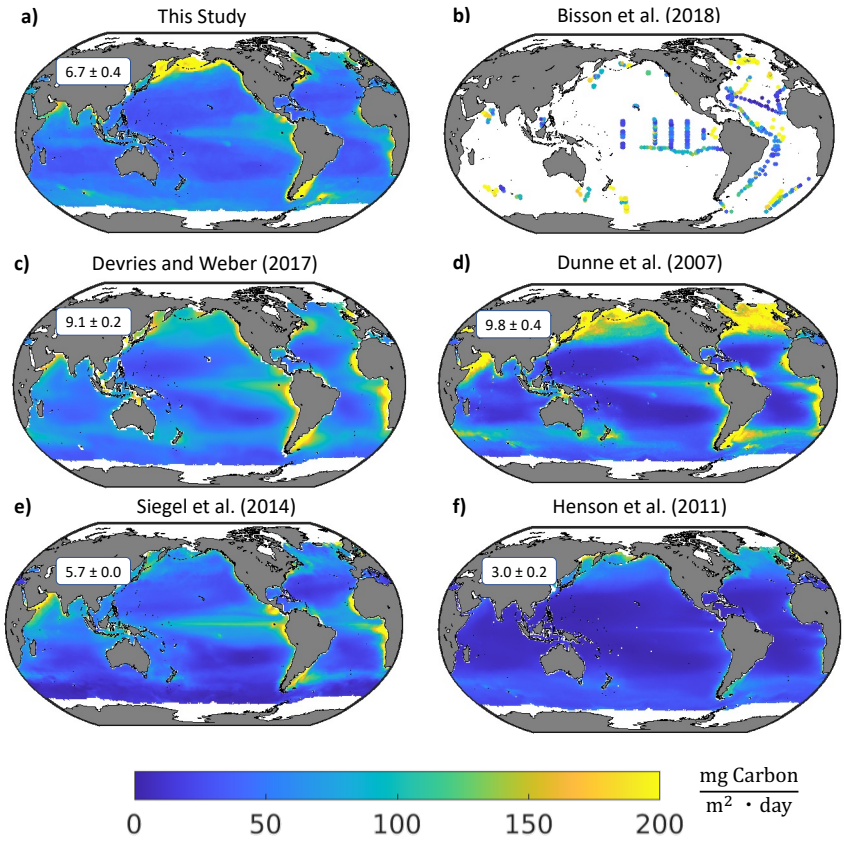

Figure 3. Annual average particle export flux (mg C m^{-2} d^{-1}) from the euphotic zone for (a) the global PSD-derived flux from this study, compared to (b) the *in situ* data of Bisson et al. (2018), (c) the steady state satellite-driven model SIMPLE-TRIM of DeVries et al. (2017), (d) the empirical model of Dunne et al. (2007), (e) the satellite-driven euphotic zone food web model Siegel et al. (2014), and (e) the empirical model of Henson et al. (2011). Annotations in each figure show the globally integrated export in Pg C y^{-1}, and the uncertainty reported by each study.

3.1.1 Spatial variability

We illustrate the main spatial differences between our and other reconstructions by considering zonally averaged export fluxes (Fig. 4). The largest export rates are observed around the equator, in the subpolar Pacific Ocean, and in the mid- to high-latitudes of the South Atlantic Ocean, while more uniform export is observed in the Indian Ocean. In all basins, the minimum export rates are generally located at the latitude of the subtropical gyres. While export is nearly symmetrical around the equator in the Pacific Ocean (Fig. 4a), in the Atlantic Ocean it dramatically increases moving from the Northern to the Southern Hemisphere (Fig. 4b). These patterns reflect a combination of open-ocean and shelf enhanced particle export. Specifically, high export in the Northern Pacific and Southern Atlantic Oceans are partly driven by large fluxes in the Bering Sea, the Sea of Okhotsk, and the Patagonian shelf. At lower latitudes, coastal upwelling systems sustain particularly high export in the northern Indian Ocean and the tropical to subtropical Atlantic.

Variations in export patterns derived with our approach (Equations 1 and 5) reflect a combination of spatially varying PSD biovolume and slope (Clements et al., 2021). Slope and biovolume are both strongly correlated to each other and overall flux (Supplementary figure S4 and S5). These two quantities generally correlate in such a way as to increase export fluxes in particle-rich productive waters, where large, rapidly sinking particles tend to be relatively more abundant than small particles, and decrease them in particle-poor oligotrophic waters where small particles dominate (Clements et al., 2021). High export in the eastern equatorial and tropical Pacific can be attributed to relatively high biovolume, with a minor contribution from PSD slope, which appears to be more uniform across the region. The picture is somewhat different in the equatorial Atlantic Ocean, where a more substantial "flattening" of the PSD suggests a more important role of large particles in driving elevated export fluxes. A similar interaction of particle abundance and size-structure dramatically intensify fluxes in the subpolar North Pacific and Southern Ocean, and to a lesser extent the subpolar Atlantic, where a relative increase in particle abundance is followed by a shift of the PSD toward large particles. In contrast, along many coastal regions, including eastern boundary upwelling systems and the Arabian Sea upwelling, increase in particle biovolume, rather than substantial changes in size structure, appears to drive enhanced export fluxes.

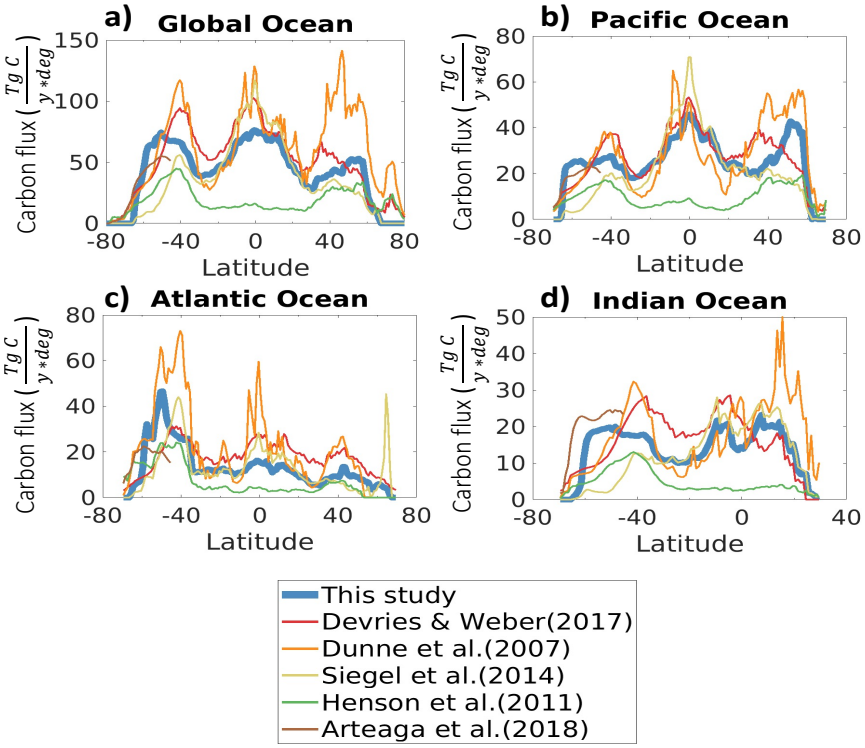

Figure 4. Zonally integrated annual mean export (Tg C y^{-1} $degree^{-1}$) for (a) the Global Ocean, (b) the Pacific Ocean, (c) the Atlantic Ocean, and (d) the Indian Ocean. Each color represents a different study, as shown in the legend (bottom).

Our reconstruction shows broad meridional patterns similar to previous estimates (Fig. 4); however, significant regional-level discrepancies remain. For example, in the low latitudes, we predict somewhat less intense equatorial export peaks and subtropical lows, compared to the estimates of Dunne et al. (2007) and Siegel et al. (2014). In this respect,

our reconstruction is more in line with the results of DeVries and Weber (2017). In the northern Pacific, we do broadly miss the transition zone as a persistent feature, however, seasonally it is present (Supplementary figure S2). Overall, in the subpolar region our estimate shows a northward shift of maximum export that is comparable to the results of Dunne et al. (2007). This is likely caused by intensification of particle fluxes in coastal waters and marginal seas, which may be related to regional processes such as more efficient nutrient recycling in shallow regions, or iron leakage from continental shelves (Nishioka et al., 2020). In the Atlantic Ocean, the gradual increase of export from northern to southern latitudes (mostly driven by high export near the coast), and the rapid increase in the Southern Ocean (caused by high export near the Patagonian shelf), are similar to the reconstruction of Henson et al. (2011), although the magnitude is larger. In the Indian Ocean, our reconstruction matches other studies at low latitudes; however, it shows a more dramatic increase in export towards the Southern Ocean sector (see also Section 3.2).

3.1.2 Seasonal cycle

The seasonal cycle of particle export is comparable to previous studies, when averaged over large-scale coherent biomes (Fig. 5). However, significant discrepancies are also revealed. In general, our seasonal cycle is more muted than previous work, suggesting weaker month-to-month variability in some regions, while other regions match previous reconstructions more closely.

Similar to other estimates, we capture well-known seasonal export pulses associated with spring phytoplankton blooms in the North Atlantic and North Pacific Oceans. Over most of the tropics, our reconstruction reveals nearly constant export through the year, and a slight asymmetry about the equator, with more pronounced seasonality in the Northern Hemisphere compared to the Southern Hemisphere. The most significant discrepancy is observed in the Southern Ocean, in particular in the Antarctic zone, where our reconstruction is substantially higher than previous estimates, with sustained export throughout winter months. We discuss this deviation in detail in Section 3.2.

When compared with other studies, our results show overall similar patterns in seasonal variability, but lower seasonality in most regions, particularly at higher latitudes (Fig. 5). The relatively muted seasonality is consistent with the weaker spatial gradients, and suggests overall weaker variations in net community production and export than previously assumed. The machine learning approach used to reconstruct the PSD relies on non-linear relationships with multiple ocean variables to reconstruct particle size distributions, which may accentuate compensatory relationships between different predictors. Surface chlorophyll, temperature, and net primary production have all been used in previous global reconstructions (Dunne et al., 2007; Henson et al., 2011; Siegel et al., 2014), but rarely together with additional variables that may be important in modulating spatial and seasonal export patterns. It is also possible that our method somewhat underestimates variability compared to previous work. As previously noted, our PSD reconstructions appear to reduce extremes in both biovolume and PSD slope (Clements et al., 2021), which may lead to underestimating variability in particle export fluxes derived from these quantities.

3.2 Southern Ocean Export

Export flux in the Antarctic zone of the Southern Ocean are substantially larger than other global reconstructions, especially during winter (Fig. 5). A regional study based on 10 years of biogeochemical Argo measurements from 2006-2014, combined with satellite-based net primary production and export algorithms, similarly suggests higher than previously reported particle fluxes throughout the region (Arteaga et al., 2018), in better agreement with our results (Fig. 6). This similarity is mostly evident in the open ocean,

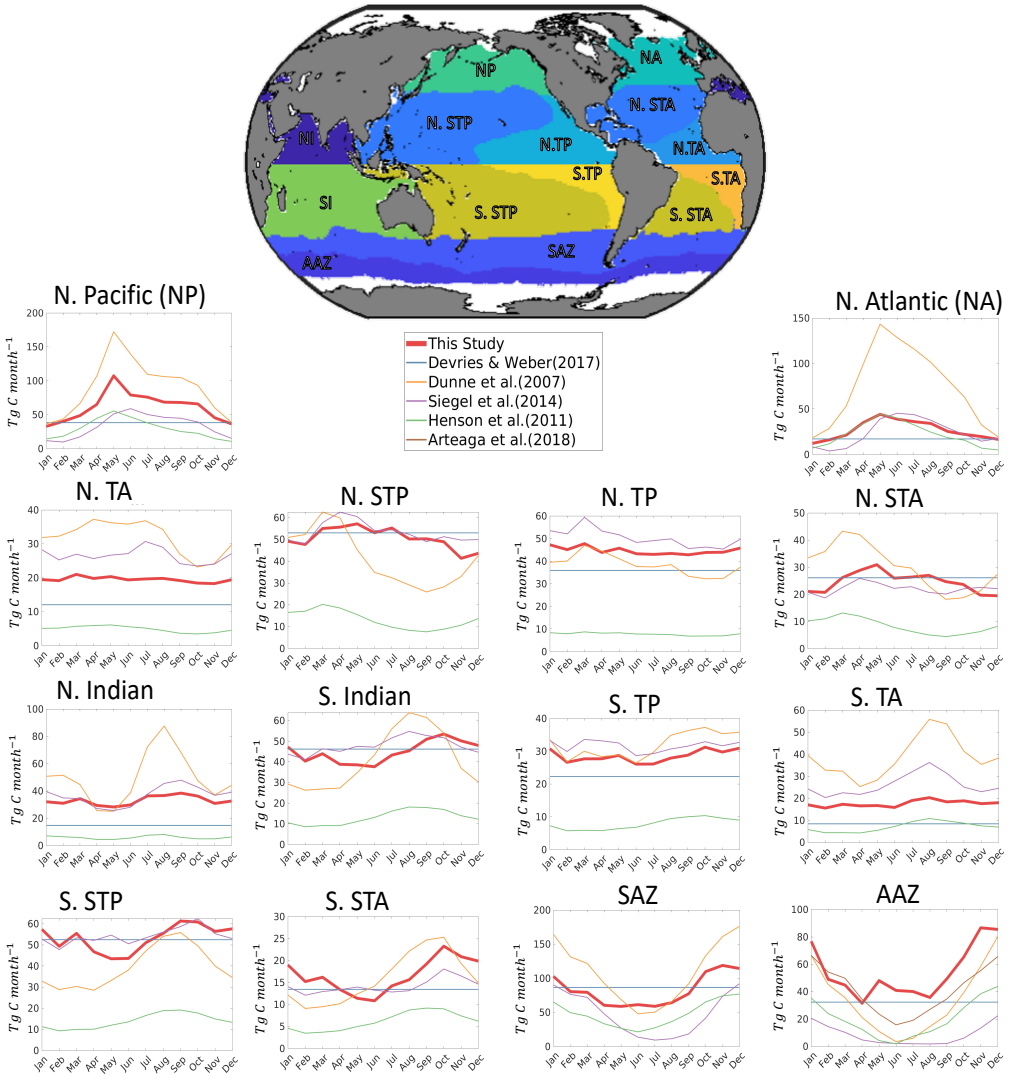

Figure 5. Annual seasonal cycle of particle flux from the euphotic zone (Tg C y^{-1}) for the regions specified in the map (top). Each line corresponds to a different estimate, as listed in the legend below the map. The same seasonal spatial mask was applied to each study. Note that the study DeVries and Weber (2017) provides annual mean export fluxes, which are shown here as horizontal lines.

and varies depending on the primary production algorithm chosen for the comparison. However, our estimate also reveals substantially higher export near landmasses, for example the Patagonian Shelf, South Georgia and the South Sandwich Islands, and the Kerguelen Plateau. Although estimates from Arteaga et al. (2018) do not show the same high flux in winter as our reconstruction, they do demonstrate that export fluxes from the Antarctic zone of the Southern Ocean likely never decrease to the nearly negligible levels shown by other global estimates (Fig. 5).

The discrepancy in export from the Antarctic zone relative to prior global estimates could arise from a combination of factors. First, observations in the Southern Ocean, particularly in winter, are scarce. This is true for both the UVP5 measurements and the climatological predictors used to reconstruct PSD (Clements et al., 2021). The UVP5

data compilation (Kiko et al., 2021) includes only two major cruises in the Southern Ocean, which only cover the months of March to May. Satellite-based reconstructions of chlorophyll and primary production from ocean color are also poorly resolved in wintertime. Other climatological variables, such nutrients and oxygen, are also the results of interpolation of fewer *in situ* observations relative to the rest of the ocean. The scarcity of observations to train the machine learning model used for the PSD reconstructions (Clements et al., 2021) results in significant uncertainty in predicted PSD and export fluxes in this region.

Second, our reconstruction reveals significant export primarily next to land masses. Proximity to land masses has been shown to increase productivity and carbon flux (Jouandet et al., 2014; Stemmann, Eloire, et al., 2008), presumably via enhanced vertical mixing and iron fertilization from sedimentary sources in otherwise high-nutrient low-chlorophyll waters (Gaiero et al., 2003). It is possible that other methods of flux reconstructions (Henson et al., 2011; Siegel et al., 2014; DeVries & Weber, 2017) underestimate this increased export, in particular during winter, when observations are scarce. Increasing the number of *in situ* particle flux and UVP5 observations from the Antarctic zone, in particular downstream of major land masses and in wintertime, could help shed light on the patterns of export and their variability in this undersampled region.

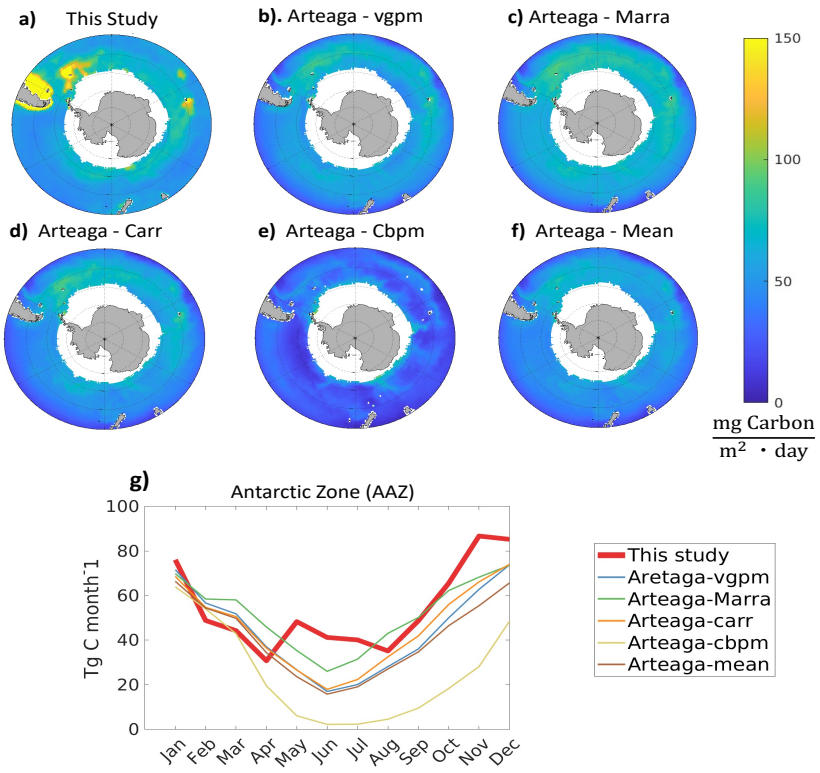

Figure 6. Southern Ocean particle export (mg C m^{-2} d^{-1}) for (a) this study, and (b-e) different data-based estimates from Arteaga et al. (2018), and (f) the mean from that study. Each data-based estimate from Arteaga et al. (2018) uses a different net primary production algorithm to derive export. (g) Seasonal cycle of export for each estimate in the Antarctic zone (shown in figure 5).

3.3 Mixed layer versus euphotic zone export

Our approach can be extended to reconstruct fluxes at any given depth in the ocean, provided that PSD observations are available (Guidi et al., 2008, 2016; Kiko et al., 2017). Because of the high vertical resolution, UVP5 observations allow to estimate PSD at multiple depths in the water column. We repeat the calculations of Clements et al. (2021) to reconstruct global PSD at the depth of the climatological wintertime mixed layer, here taken as the deepest mixed layer from an Argo-based data product (Johnson et al., 2012). We then use this depth as the new export horizon for the flux calculations (Equation 5), and compare the results to the export from the euphotic zone (Fig. 3).

We find that, globally integrated, the particulate carbon export from the mixed layer is 9.4 ±1.1 PgC/y, i.e., about 3 Pg/year larger than the global export from the euphotic zone. This estimate is slightly lower than observational estimates of organic carbon export and annual net community production from the same depth horizon (Emerson, 2013).

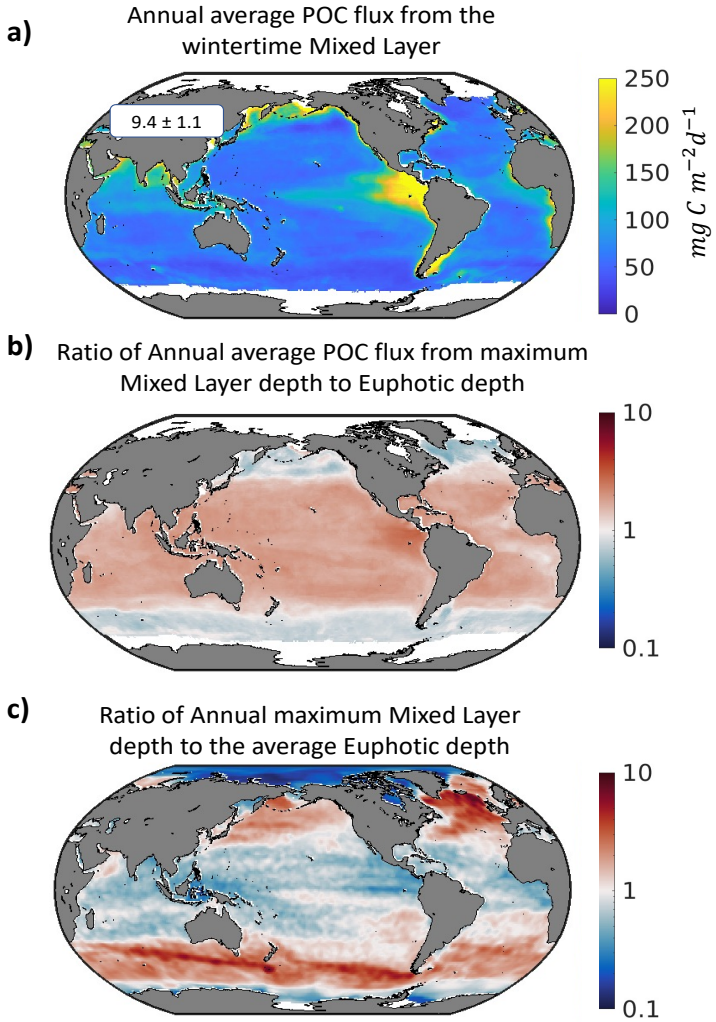

Figure 7. (a) Annual mean particle export (mg C m^{-2} d^{-1}) from the maximum mixed layer depth. Total export is 9.4 PgC/y. (b) Ratio of the export from the maximum mixed layer depth to the export from the euphotic zone. (c) Ratio of the maximum mixed layer depth to the euphotic zone depth.

Overall, export from the wintertime mixed layer follows broad spatial patterns similar to the export from the euphotic zone (Fig. 7a). However, tropics and subtropics show larger export fluxes at the mixed layer depth (locally, up to a few times), while high latitudes show overall weaker export fluxes (Fig. 7b). The low-latitude intensification of mixed layer particle fluxes is similar in all ocean basins, and more than compensates for the reduction at high latitudes (Supplementary Fig. S6), thus producing an overall larger export from this horizon. Because of this low-latitude intensification, export from the mixed layer shows stronger gradients between the tropics and high latitudes. Gradients between the equatorial export peak and the subtropical export low are also intensified. Finally, export from the mixed layer in the Southern Ocean is substantially depressed compared to export from the euphotic zone.

Differences between euphotic zone and mixed layer export can be best interpreted by considering the different depth of these horizons (Palevsky & Doney, 2018). The depth of the maximum mixed layer is shallower than the euphotic zone in the tropics and subtropics, and is deeper in high latitudes (Fig. 7c). This suggests that shallower export horizons are generally characterized by higher fluxes than deeper export horizons, likely because of remineralization of particles in the upper layers of the ocean. Specifically, we identify three main latitudinal bands with different horizon depths and export patterns, roughly corresponding to tropics and subtropics, mid-latitudes, and subpolar regions.

Over most of the tropics and the subtropics, the maximum wintertime mixed layer is shallower on average than the climatological euphotic zone (blue colors in Fig. 7c). Here, particle remineralization between the wintertime mixed layer and the euphotic zone depth reduces export from the latter horizon, suggesting net heterotrophy in the deeper layers of the euphotic zone. Over subpolar regions, the wintertime mixed layer is deeper on average than the climatological euphotic zone. Here, export fluxes reach maximum values within the euphotic zone, and decrease below it following remineralization. Finally, over most of mid-latitudes, the wintertime mixed layer is deeper on average than the climatological euphotic zone. However, export fluxes from the mixed layer and euphotic zone are very similar in magnitude, suggesting a close seasonal compensations between enhanced euphotic zone fluxes when this horizon is found above the wintertime mixed layer, and reduced euphotic zone fluxes when it is found below it.

Ultimately, differences in export between the euphotic zone and the wintertime mixed layer are important when considering the role of the biological pump for carbon sequestration (Palevsky & Doney, 2018). Export below the wintertime mixed layer removes carbon from contact with the atmosphere for time scales longer than one year. Our results suggest that more carbon is sequestered below the wintertime mixed layer than leaves the euphotic zone.

3.4 Caveats to our approach

There are multiple sources of uncertainty and inherent limitations that could affect our estimates and call for further work. Our method relies on global PSD reconstructions from UVP5 observations, as well as *in situ* particle flux measurements, both of which are spatially and temporally limited. This in turns limits the ability of our approach to (1) obtain an accurate climatological picture of PSD and fluxes, and (2) extrapolate local observations to larger regions and other times of the year. In particular, about forty-three percent of monthly particle flux observations contain only one measurement, and entire ocean basins are represented by a handful of measurements (Fig. 2b). While more widely distributed than flux measurements, UVP5 observations are also characterized by large gaps in space and time (Kiko et al., 2021). As noted in the companion paper (Clements et al., 2021), regional correlations between environmental properties and PSD observations from UVP5 may not be well captured by extrapolation with a machine learning algorithm trained on data from different regions, especially when non-linear relation-

ships between variables become important. Expanding the coverage of *in situ* PSD and fluxes, in particular in under-sampled regions characterized by large variability, such as the Southern Ocean, would improve the robustness of our estimates, and shed additional light on regional export patterns not captured by previous work.

The conversion of PSD to export flux encapsulated by Equations 1 and 5 also suffers from inherent limitations. Converting standing stocks of particles from UVP5 observations to sinking carbon flux using size-dependent relationships assumes that (1) all particles of a given size have the same carbon content, and (2) they all sink at a similar speed proportional to their size. Known biases exist with both assumptions. For example, densely packed fecal pellets often contain more carbon and sink faster than heterogeneous aggregates and marine snow of the same size (Alldredge, 1998). Furthermore, we assume globally uniform relationships between particle size, sinking speed, and carbon content. However, these relationships remain quite uncertain (Alldredge, 1998; Stemmann & Boss, 2012; Cael et al., 2021), and are likely to depend on region and time of the year, reflecting variable particle characteristics and underlying ecological processes.

We suggest that our approach, which optimizes carbon content and sinking velocity parameters against *in situ* particle fluxes, limits the effect of these uncertainties. More work combining *in situ* and optical measurements should focus on constraining these quantities and their regional and temporal variability. Future studies could also improve our approach by distinguishing living and non-living particles, particle type, and composition, e.g., by analysis of UVP5 images or other optical methods in conjunction with *in situ* particle samples.

4 Conclusions and future work

We provide a new, data-constrained estimate of particle export fluxes by combining global reconstructions of PSD from UVP5 observations and *in situ* export flux measurements. Our reconstruction captures regional and seasonal variability in reconstructed fluxes, and demonstrates the power of statistical machine learning methods applied to in situ UVP5 observations. The approach also allows reconstruction of export fluxes from any given depth; here, we focus on spatially variable euphotic zone and mixed layer depths, highlighting the importance of the choice of export horizon (Palevsky & Doney, 2018), and paving the way to fully three-dimensional particle flux reconstructions in the ocean interior.

We obtain a global particle export flux of 6.7 $\pm$ 0.4 PgC/year from the euphotic zone, in line with previous work, although with significant regional and temporal differences. Our results suggest weaker spatial and seasonal variability compared to previous studies, in particular in the open ocean, and highlight the importance of coastal waters and marginal seas for export at high latitudes. We also capture similar patterns of high latitude seasonal blooms in the Northern Hemisphere as previous studies, but less variable flux in the tropical to subtropical ocean, and substantially higher year-round export in the Southern Ocean, in better agreement with regional estimates (Arteaga et al., 2018). Results from the Southern Ocean suggest that processes that sustain elevated fluxes, in particular in wintertime, may not be completely captured by other global reconstructions, and that waters downstream of coasts and islands may harbor a significant source of carbon export to the deep ocean, which is only partially captured in one other reconstruction (Dunne et al., 2007).

The statistical nature of our machine learning approach does not directly reveal mechanisms behind export fluxes. However, we are able to highlight globally coherent patterns, and the relative importance of particle abundance and size structure in driving export. Total particle biovolume and the PSD slope are correlated in such a way to act synergistically on particle fluxes (Clements et al., 2021); consistently, higher fluxes

are reconstructed in regions with larger particle biovolume and "flatter" slopes. We also suggest distinct deviations from these patterns, for example in the tropical and northern subtropical Pacific Ocean, where high abundance of all particles, rather than dominance of large relative to small particles, appears to drive elevated export.

We illustrate the ability of our method to obtain particulate organic carbon fluxes at multiple depth by reconstructing and comparing carbon export from the euphotic zone and the wintertime mixed layer depth. Export from the mixed layer is overall stronger than export from the euphotic zone in low and mid latitudes, and weaker in high latitudes, driving a significantly larger export of 9.4 $\pm$1.1 PgC/year. Three-dimensional reconstructions of particle fluxes would allow a closer investigation of the processes controlling export changes with depth and their implications for particle transfer efficiency and carbon sequestration.

We identified sources of uncertainty and limitations in our approach that should be addressed in future work. There remain areas of the ocean and times of the year with limited UVP5 observations and, critically, *in situ* flux measurements, driving uncertainty in both the PSD and flux reconstructions. As UVP5 observations increase in number, our analysis can be refined, for example by expanding comparison with particle flux data (Mouw et al., 2016). The machine learning algorithm used to reconstruct global PSD appears to reduce some of the observed variability (Clements et al., 2021), which in turn may translate in a reduced range for reconstructed export fluxes. Testing different machine learning methods could help reducing this bias. While we assumed globally uniform carbon content and sinking speed parameters, they could be parameterized to reflect regional variability and particle types. Finally, while analysis of correlations between flux reconstructions and environmental predictors suggests mechanistic linkages, the statistical nature of the approach cannot reveal the specific underlying processes and their dynamics.

Comparison of our flux reconstructions with previous work reveals inherent strength and weakness of various approaches, and suggest a systematic uncertainty in our current ability to constrain export with both empirical and mechanistic methods. We echo suggestions to combine flux estimates from multiple approaches in studies of the biological pump (Quay et al., 2020), focusing the attention on regions and periods of high discrepancy.

The three-dimensional nature of UVP5 observations opens the door to fully three-dimensional reconstructions of particle export fluxes. This will greatly benefit from particle flux compilations that span the full depth of the ocean (Mouw et al., 2016), and that harmonize discrepancies between different flux measurement methods (Bisson et al., 2018). Ongoing deployments of UVP instruments, including on Argo floats, will rapidly increase the number of PSD observations with high vertical resolution. In turn, three-dimensional reconstructions of export will enable a better characterization the ocean's ability to sequester carbon, and, in combination with models (DeVries & Weber, 2017; Siegel et al., 2014), a better understanding of the processes behind the ocean's biological pump.

Acknowledgments

This material is based upon work supported by the U.S. National Science Foundation under grants No. OCE-1635632 and OCE-1847687. D.B. acknowledges support from the Alfred P. Sloan Foundation, and computational support by the Extreme Science and Engineering Discovery Environment (XSEDE) through allocation TG-OCE17001. A.M.P.M acknowledges support from NSF Award No. 1654663. T.W. was supported by NSF award OCE-1635414. RK acknowledges support via the BMBF funded project CUSCO, the EU project TRIATLAS (European Union's Horizon 2020 programme, grant agreement No 817578) and a "Make Our Planet Great Again" grant of the ANR within the "Programme d'Investissements d'Avenir"; reference "ANR-19-MPGA-0012". Data generated

by this analysis has been uploaded to BCO-DMO, DOI:10.26008/1912/bco-dmo.856942.1. The individual UVP5 profiles used to generate the reconstructions can be obtained on the EcoTaxa website https://ecotaxa.obs-vlfr.fr/part/.

References

Alldredge, A. (1998). The carbon, nitrogen and mass content of marine snow as a function of aggregate size. *Deep-Sea Research Part I: Oceanographic Research Papers*, *45*(4-5), 529–541. doi: 10.1016/S0967-0637(97)00048-4

Arteaga, L., Haëntjens, N., Boss, E., Johnson, K. S., & Sarmiento, J. L. (2018). Assessment of Export Efficiency Equations in the Southern Ocean Applied to Satellite-Based Net Primary Production. *Journal of Geophysical Research: Oceans*, *123*(4), 2945–2964. doi: 10.1002/2018JC013787

Bianchi, D., Stock, C., Galbraith, E. D., & Sarmiento, J. L. (2013). Diel vertical migration: Ecological controls and impacts on the biological pump in a one-dimensional ocean model. *Global Biogeochemical Cycles*, *27*(2), 478–491. Retrieved from `https://agupubs.onlinelibrary.wiley.com/doi/abs/10.1002/gbc.20031` doi: https://doi.org/10.1002/gbc.20031

Bianchi, D., Weber, T. S., Kiko, R., & Deutsch, C. (2018). Global niche of marine anaerobic metabolisms expanded by particle microenvironments. *Nature Geoscience*, 1–6. Retrieved from `http://dx.doi.org/10.1038/s41561-018-0081-0` doi: 10.1038/s41561-018-0081-0

Bisson, K. M., Siegel, D. A., DeVries, T., Cael, B. B., & Buesseler, K. O. (2018). How Data Set Characteristics Influence Ocean Carbon Export Models. *Global Biogeochemical Cycles*, *32*(9), 1312–1328. doi: 10.1029/2018GB005934

Bourne, H. L., Bishop, J. K., Wood, T. J., Loew, T. J., & Liu, Y. (2019). Carbon Flux Explorer optical assessment of C, N and P fluxes. *Biogeosciences*, *16*(6), 1249–1264. doi: 10.5194/bg-16-1249-2019

Boyd, P. W., Claustre, H., Levy, M., Siegel, D. A., & Weber, T. (2019). Multi-faceted particle pumps drive carbon sequestration in the ocean. *Nature*, *568*(7752), 327–335. Retrieved from `https://doi.org/10.1038/s41586-019-1098-2` doi: 10.1038/s41586-019-1098-2

Buesseler, K., Antia, A., Chen, M., Fowler, S., Gardner, W., Gustafsson, O., ... Trull, T. (2007, 05). An assessment of the use of sediment traps for estimating upper ocean particle fuxes. *Journal of Marine Research*, *65*. doi: 10.1357/002224007781567621

Buesseler, K. O., & Boyd, P. W. (2009). Shedding light on processes that control particle export and flux attenuation in the twilight zone of the open ocean. *Limnology and Oceanography*, *54*(4), 1210–1232. doi: 10.4319/lo.2009.54.4.1210

Buesseler, K. O., Boyd, P. W., Black, E. E., & Siegel, D. A. (2020). Metrics that matter for assessing the ocean biological carbon pump. *Proceedings of the National Academy of Sciences of the United States of America*, *117*(18), 9679–9687. doi: 10.1073/pnas.1918114117

Cael, B., Cavan, E. L., & Britten, G. L. (2021). Reconciling the size-dependence of marine particle sinking speed. *Geophysical Research Letters*, *48*(5), e2020GL091771.

Carlson, C. A., Ducklow, H. W., & Michaels, A. F. (1994). Annual flux of dissolved organic carbon from the euphotic zone in the northwestern sargasso sea. *Nature*, *371*(6496), 405–408.

Clements, D., Yang, S., Weber, T., McDonnell, A., Kiko, R., Stemmann, L., & Bianchi, D. (2021). Constraining the ocean's biological pump with in situ optical observations and supervised learning. part 1: particle size distributions. *In Review for Global Biogeochemical Cycles*.

Cram, J. A., Weber, T., Leung, S. W., McDonnell, A. M., Liang, J. H., & Deutsch,

C. (2018). The Role of Particle Size, Ballast, Temperature, and Oxygen in the Sinking Flux to the Deep Sea. *Global Biogeochemical Cycles*, *32*(5), 858–876. doi: 10.1029/2017GB005710

Dall'Olmo, G., Dingle, J., Polimene, L., Brewin, R. J., & Claustre, H. (2016). Substantial energy input to the mesopelagic ecosystem from the seasonal mixed-layer pump. *Nature Geoscience*, *9*(11), 820–823. doi: 10.1038/ngeo2818

DeVries, T., Holzer, M., & Primeau, F. (2017). Recent increase in oceanic carbon uptake driven by weaker upper-ocean overturning. *Nature*, *542*(7640), 215–218. Retrieved from `http://dx.doi.org/10.1038/nature21068` doi: 10.1038/nature21068

DeVries, T., Primeau, F., & Deutsch, C. (2012). The sequestration efficiency of the biological pump. *Geophysical Research Letters*, *39*(13).

DeVries, T., & Weber, T. (2017). The export and fate of organic matter in the ocean: New constraints from combining satellite and oceanographic tracer observations. *Global Biogeochemical Cycles*, *31*(3), 535–555. doi: 10.1002/2016GB005551

Dunne, J. P., Sarmiento, J. L., & Gnanadesikan, A. (2007). A synthesis of global particle export from the surface ocean and cycling through the ocean interior and on the seafloor. *Global Biogeochemical Cycles*, *21*(4), 1–16. doi: 10.1029/2006GB002907

Emerson. (2013). Global Biogeochemical Cycles the biological carbon flux in the ocean. *Global Biogeochemical Cycles*, 14–28. doi: 10.1002/2013GB004680

Fontanez, K. M., Eppley, J. M., Samo, T. J., Karl, D. M., & DeLong, E. F. (2015). Microbial community structure and function on sinking particles in the north pacific subtropical gyre. *Frontiers in microbiology*, *6*, 469.

Forest, A., Stemmann, L., Picheral, M., Burdorf, L., Robert, D., Fortier, L., & Babin, M. (2012). Size distribution of particles and zooplankton across the shelf-basin system in southeast Beaufort Sea: Combined results from an Underwater Vision Profiler and vertical net tows. *Biogeosciences*, *9*(4), 1301–1320. doi: 10.5194/bg-9-1301-2012

Gaiero, D., Probst, J.-L., Depetris, P., Bidart, S., & Leleyter, L. (2003). Iron and other transition metals in patagonian riverborne and windborne materials: geochemical control and transport to the southern south atlantic ocean. *Geochimica et Cosmochimica Acta*, *67*(19), 3603-3623. Retrieved from `https://www.sciencedirect.com/science/article/pii/S0016703703002114` doi: https://doi.org/10.1016/S0016-7037(03)00211-4

Guidi, L., Chaffron, S., Bittner, L., Eveillard, D., Larhlimi, A., Roux, S., ... Gorsky, G. (2016). Plankton networks driving carbon export in the oligotrophic ocean. *Nature*, *532*(7600), 465–470. Retrieved from `http://dx.doi.org/10.1038/nature16942` doi: 10.1038/nature16942

Guidi, L., Jackson, G. A., Stemmann, L., Miquel, J. C., Picheral, M., & Gorsky, G. (2008). Relationship between particle size distribution and flux in the mesopelagic zone. *Deep-Sea Research Part I: Oceanographic Research Papers*, *55*(10), 1364–1374. doi: 10.1016/j.dsr.2008.05.014

Guidi, L., Legendre, L., Reygondeau, G., Uitz, J., Stemmann, L., & Henson, S. A. (2015, jul). A new look at ocean carbon remineralization for estimating deepwater sequestration. *Global Biogeochemical Cycles*, *29*(7), 1044–1059. Retrieved from `http://doi.wiley.com/10.1002/2014GB005063` doi: 10.1002/2014GB005063

Guidi, L., Stemmann, L., Jackson, G. A., Ibanez, F., Claustre, H., Legendre, L., ... Gorsky, G. (2009). Effects of phytoplankton community on production, size and export of large aggregates: A world-ocean analysis. *Limnology and Oceanography*, *54*(6), 1951–1963. doi: 10.4319/lo.2009.54.6.1951

Henson, S. A., Sanders, R., Madsen, E., Morris, P. J., Le Moigne, F., & Quartly, G. D. (2011). A reduced estimate of the strength of the ocean's bi-

682 ological carbon pump. *Geophysical Research Letters*, *38*(4), 10–14. doi:
683 10.1029/2011GL046735
684 Honjo, S., Manganini, S. J., Krishfield, R. A., & Francois, R. (2008). Partic-
685 ulate organic carbon fluxes to the ocean interior and factors controlling
686 the biological pump: A synthesis of global sediment trap programs since
687 1983. *Progress in Oceanography*, *76*(3), 217-285. Retrieved from `https://`
688 `www.sciencedirect.com/science/article/pii/S0079661108000025` doi:
689 https://doi.org/10.1016/j.pocean.2007.11.003
690 Johnson, G. C., Schmidtko, S., & Lyman, J. M. (2012). Relative contributions of
691 temperature and salinity to seasonal mixed layer density changes and horizon-
692 tal density gradients. *Journal of Geophysical Research: Oceans*, *117*(4). doi:
693 10.1029/2011JC007651
694 Jouandet, M. P., Jackson, G. A., Carlotti, F., Picheral, M., Stemmann, L., & Blain,
695 S. (2014). Rapid formation of large aggregates during the spring bloom of Ker-
696 guelen Island: Observations and model comparisons. *Biogeosciences*, *11*(16),
697 4393–4406. doi: 10.5194/bg-11-4393-2014
698 Karl, D., Knauer, G., Martin, J., & Ward, B. (1984). Bacterial chemolithotrophy in
699 the ocean is associated with sinking particles. *Nature*, *309*(5963), 54–56.
700 Kiko, R., Biastoch, A., Brandt, P., Cravatte, S., Hauss, H., Hummels, R., ... Stem-
701 mann, L. (2017). Biological and physical influences on marine snowfall at the
702 equator. *Nature Geoscience*, *10*(11), 852–858. doi: 10.1038/NGEO3042
703 Kiko, R., Brandt, P., Christiansen, S., Faustmann, J., Kriest, I., Rodrigues, E., ...
704 Hauss, H. (2020, 5). Zooplankton-mediated fluxes in the eastern tropical north
705 atlantic. *Frontiers in Marine Science*, *7*. doi: 10.3389/fmars.2020.00358
706 Kiko, R., Picheral, M., Antoine, D., Babin, M., Berline, L., Biard, T., ... Stem-
707 mann, L. (2021). The global marine particle size distribution dataset obtained
708 with the underwater vision profiler 5 - version 1. *PANGAEA*.
709 Kriest, I. (2002). Different parameterizations of marine snow in a 1D-model and
710 their influence on representation of marine snow, nitrogen budget and sedimen-
711 tation. *Deep-Sea Research Part I: Oceanographic Research Papers*, *49*(12),
712 2133–2162. doi: 10.1016/S0967-0637(02)00127-9
713 Kwon, E. Y., Primeau, F., & Sarmiento, J. L. (2009). The impact of remineraliza-
714 tion depth on the air–sea carbon balance. *Nature Geoscience*, *2*(9), 630–635.
715 Laws, E. A., D'Sa, E., & Naik, P. (2011). Simple equations to estimate ratios of new
716 or export production to total production from satellite-derived estimates of sea
717 surface temperature and primary production. *Limnology and Oceanography:*
718 *Methods*, *9*(DECEMBER), 593–601. doi: 10.4319/lom.2011.9.593
719 Le Gland, G., Aumont, O., & Mémery, L. (2019). An estimate of thorium 234
720 partition coefficients through global inverse modeling. *Journal of Geo-*
721 *physical Research: Oceans*, *124*(6), 3575-3606. Retrieved from `https://`
722 `agupubs.onlinelibrary.wiley.com/doi/abs/10.1029/2018JC014668` doi:
723 https://doi.org/10.1029/2018JC014668
724 Longhurst, A., Bedo, A., Harrison, W., Head, E., & Sameoto, D. (1990). Verti-
725 cal flux of respiratory carbon by oceanic diel migrant biota. *Deep Sea Research*
726 *Part A. Oceanographic Research Papers*, *37*(4), 685–694.
727 Morel, A., Huot, Y., Gentili, B., Werdell, P. J., Hooker, S. B., & Franz, B. A.
728 (2007). Examining the consistency of products derived from various ocean
729 color sensors in open ocean (Case 1) waters in the perspective of a multi-
730 sensor approach. *Remote Sensing of Environment*, *111*(1), 69–88. doi:
731 10.1016/j.rse.2007.03.012
732 Mouw, C. B., Barnett, A., McKinley, G. A., Gloege, L., & Pilcher, D. (2016). Global
733 ocean particulate organic carbon flux merged with satellite parameters. *Earth*
734 *System Science Data*, *8*(2), 531–541.
735 Nishioka, J., Obata, H., Ogawa, H., Ono, K., Yamashita, Y., Lee, K., ... Yasuda,
736 I. (2020). Subpolar marginal seas fuel the North Pacific through the interme-

diate water at the termination of the global ocean circulation. *Proceedings of the National Academy of Sciences of the United States of America*, *117*(23), 12665–12673. doi: 10.1073/pnas.2000658117

Omand, M. M., D'Asaro, E. A., Lee, C. M., Perry, M. J., Briggs, N., Cetinić, I., & Mahadevan, A. (2015). Eddy-driven subduction exports particulate organic carbon from the spring bloom. *Science*, *348*(6231), 222–225. doi: 10.1126/science.1260062

Palevsky, H. I., & Doney, S. C. (2018). How Choice of Depth Horizon Influences the Estimated Spatial Patterns and Global Magnitude of Ocean Carbon Export Flux. *Geophysical Research Letters*, *45*(9), 4171–4179. doi: 10.1029/2017GL076498

Picheral, M., Guidi, L., Stemmann, L., Karl, D. M., Iddaoud, G., & Gorsky, G. (2010). The underwater vision profiler 5: An advanced instrument for high spatial resolution studies of particle size spectra and zooplankton. *Limnology and Oceanography: Methods*, *8*(SEPT), 462–473. doi: 10.4319/lom.2010.8.462

Quay, P., Emerson, S., & Palevsky, H. (2020). Regional Pattern of the Ocean's Biological Pump Based on Geochemical Observations. *Geophysical Research Letters*, *47*(14), 1–10. doi: 10.1029/2020GL088098

Riley, J. S., Sanders, R., Marsay, C., Le Moigne, F. A., Achterberg, E. P., & Poulton, A. J. (2012). The relative contribution of fast and slow sinking particles to ocean carbon export. *Global Biogeochemical Cycles*, *26*(1), 1–10. doi: 10.1029/2011GB004085

Robinson, C., Steinberg, D. K., Anderson, T. R., Aristegui, J., Carlson, C. A., Frost, J. R., ... others (2010). Mesopelagic zone ecology and biogeochemistry–a synthesis. *Deep Sea Research Part II: Topical Studies in Oceanography*, *57*(16), 1504–1518.

Séférian, R., Berthet, S., Yool, A., Palmieri, J., Bopp, L., Tagliabue, A., ... others (2020). Tracking improvement in simulated marine biogeochemistry between cmip5 and cmip6. *Current Climate Change Reports*, 1–25.

Siegel, D. A., Buesseler, K. O., Behrenfeld, M. J., Benitez-Nelson, C. R., Boss, E., Brzezinski, M. A., ... Steinberg, D. K. (2016). Prediction of the export and fate of global ocean net primary production: The exports science plan. *Frontiers in Marine Science*, *3*(MAR), 1–10. doi: 10.3389/fmars.2016.00022

Siegel, D. A., Buesseler, K. O., Doney, S. C., Sailley, S. F., Behrenfeld, M. J., & Boyd, P. W. (2014). Global assessment of ocean carbon export by combining satellite observations and food-web models. *Global Biogeochemical Cycles*, *28*(3), 181–196. doi: 10.1002/2013GB004743

Smayda, T. J. (1970). The Suspension and sinking of phytoplankton in the sea. *Oceanography Marine Biology, Annual Review*(8), 353–414.

Steinberg, D. K., Carlson, C. A., Bates, N. R., Goldthwait, S. A., Madin, L. P., & Michaels, A. F. (2000). Zooplankton vertical migration and the active transport of dissolved organic and inorganic carbon in the sargasso sea. *Deep Sea Research Part I: Oceanographic Research Papers*, *47*(1), 137–158.

Stemmann, L., & Boss, E. (2012). Plankton and Particle Size and Packaging: From Determining Optical Properties to Driving the Biological Pump. *Annual Review of Marine Science*, *4*(1), 263–290. Retrieved from `http://www.annualreviews.org/doi/10.1146/annurev-marine-120710-100853` doi: 10.1146/annurev-marine-120710-100853

Stemmann, L., Eloire, D., Sciandra, A., Jackson, G., Guidi, L., Picheral, M., & Gorsky, G. (2008). Volume distribution for particles between 3.5 to 2000 μm in the upper 200 m region of the South Pacific Gyre. *Biogeosciences Discussions*, *5*, 299–310. doi: 10.5194/bgd-4-3377-2007

Stemmann, L., Jackson, G. A., & Ianson, D. (2004). A vertical model of particle size distributions and fluxes in the midwater column that includes biological and physical processes - Part I: Model formulation. *Deep-Sea*

Research Part I: Oceanographic Research Papers, *51*(7), 865–884. doi: 10.1016/j.dsr.2004.03.001

Stemmann, L., Youngbluth, M., Robert, K., Hosia, A., Picheral, M., Paterson, H., ... Gorsky, G. (2008). Global zoogeography of fragile macrozooplankton in the upper 100-1000 m inferred from the underwater video profiler. *ICES Journal of Marine Science*, *65*(3), 433–442. doi: 10.1093/icesjms/fsn010

Stukel, M. R., Aluwihare, L. I., Barbeau, K. A., Chekalyuk, A. M., Goericke, R., Miller, A. J., ... Landry, M. R. (2017). Mesoscale ocean fronts enhance carbon export due to gravitational sinking and subduction. *Proceedings of the National Academy of Sciences*, *114*(6), 1252–1257. Retrieved from `http://www.pnas.org/lookup/doi/10.1073/pnas.1609435114` doi: 10.1073/pnas.1609435114

Turner, J. T. (2015). Zooplankton fecal pellets, marine snow, phytodetritus and the ocean's biological pump. *Progress in Oceanography*, *130*, 205–248.

Volk, T., & Hoffert, M. I. (1985). Ocean carbon pumps: Analysis of relative strengths and efficiencies in ocean-driven atmospheric co2 changes. In *The carbon cycle and atmospheric co2: Natural variations archean to present* (p. 99-110). American Geophysical Union (AGU). Retrieved from `https://agupubs.onlinelibrary.wiley.com/doi/abs/10.1029/GM032p0099` doi: https://doi.org/10.1029/GM032p0099

Weber, T., Cram, J. A., Leung, S. W., DeVries, T., & Deutsch, C. (2016). Deep ocean nutrients imply large latitudinal variation in particle transfer efficiency. *Proceedings of the National Academy of Sciences of the United States of America*, *113*(31), 8606–8611. doi: 10.1073/pnas.1604414113